# Mesoscopic Undulations and Thickness Fluctuations in Lipid Bilayers from Molecular Dynamics Simulations

Erik Lindahl and Olle Edholm
Theoretical Physics, Royal Institute of Technology, SE-100 44 Stockholm, Sweden

ABSTRACT Molecular dynamics simulations of fully hydrated Dipalmitoylphosphatidylcholine bilayers, extending temporal and spatial scales by almost one order of magnitude, are presented. The present work reaches system sizes of 1024 lipids and times 10–60 ns. The simulations uncover significant dynamics and fluctuations on scales of several nanoseconds, and enable direct observation and spectral decomposition of both undulatory and thickness fluctuation modes. Although the former modes are strongly damped, the latter exhibit signs of oscillatory behavior. From this, it has been possible to calculate mesoscopic continuum properties in good agreement with experimental values. A bending modulus of $4 \times 10^{-20}$ J, bilayer area compressibility of 250–300 mN/m, and mode relaxation times in the nanosecond range are obtained. The theory of undulatory motions is revised and further extended to cover thickness fluctuations. Finally, it is proposed that thickness fluctuations is the explanation to the observed system-size dependence of equilibrium-projected area per lipid.

## INTRODUCTION

Lipid bilayers play important roles in cells as barriers for maintaining concentrations and as matrices to support membrane proteins. Their physical properties have been studied extensively (Bloom et al., 1991), showing the importance of membrane dynamics to the insertion of proteins and direct transport of small molecules (Gennis, 1989). The motions in membranes range from conformational transitions of the lipid hydrocarbon tails on picosecond scales to bending of 10-$\mu$m-sized patches extending to several milliseconds. The former region is accessible through spectroscopic methods (König and Sackmann, 1996), whereas the latter can be studied by microscopy (Evans, 1991). Between these domains there is a gap, the bridging of which is an important task for the understanding of how collective mesoscopic motion emerges from microscopic atomic interactions. Part of this interest comes from the observation that biological membranes are not rigid, but behave more like liquid crystals. They exhibit a very high flexibility, which enables thermally excited undulatory and peristaltic (thickness fluctuation) motions (Safran, 1994). This is essential for many of their biological properties, e.g., the extreme ability of cells like erythrocytes to change shape and the repulsive forces between interacting bilayers (Israelachveli and Wennerström, 1990). The physical basis and dynamics for many of these processes is to be found on this intermediate scale.

During the last decade, realistic atomic-level computer simulation has evolved as a complementary technique (Egberts and Berendsen, 1988) in the study of bilayers. Although such methods have made substantial progress during the last few years (Pastor, 1994; Tu et al., 1996; Tieleman et al., 1997), the available computing power has confined this to fairly small systems and time scales, below the mesoscopic realm.

To better understand the dynamics in this region, we have performed computer simulations of bilayer systems consisting of 64, 256, and 1024 Dipalmitoylphosphatidylcholine (DPPC) lipids with additional water, reaching a linear system size of 20 nm and over 120,000 atoms. The two larger systems were simulated for 10 ns, whereas the smallest was run for 60 ns. This significantly extends both the spatial and temporal scales of bilayer simulations and enables direct observation of the transition to mesoscopic phenomena like bilayer undulations and thickness fluctuations. It also makes it possible to calculate continuum properties as bending modulus, surface compressibility, and mode relaxation times in good agreement with experiment and with mesoscopic models. Further, this enables a direct test of the suggestion that finite size effects (Feller and Pastor, 1996) reduce the projected area per lipid in small systems.

## METHODS

### Forcefield and structure

The parameters of the forcefield used for the simulations have been described in detail (Berger et al., 1997) and shown to accurately reproduce experimental quantities like volume/lipid (Nagle and Wiener, 1988) and order parameters (Seelig and Seelig, 1974). United atoms were used for the $CH_2$/$CH_3$ groups in the hydrocarbon tails, reducing the number of atoms per lipid to 50. Atomic charges were taken from ab initio quantum mechanical calculations (Chiu et al., 1995). The headgroup Lennard–Jones parameters used were taken from the optimized potentials for liquid simulations forcefield (Jorgensen and Tirado-Rives, 1988), and the tail parameters the ones determined by Berger et al. (1997). 1,4 electrostatic interactions were reduced a factor of 2 and 1,4 Lennard–Jones interactions a factor of 8. Bond rotations in the carbon tails were modeled with Ryckaert–Bellemans dihedrals (Ryckaert et al., 1977) and the corresponding 1,4 interactions removed.

The initial structures were created by placing equal numbers of lipid molecules from an earlier simulation in two layers with 3-nm separation, using periodic boundary conditions. The position of each lipid was defined

*Received for publication 27 December 1999 and in final form 3 April 2000.*
Address reprint requests to Dr. Olle Edholm, Royal Institute of Technology, Theoretical Physics, SE-100 44 Stockholm, Sweden. Tel.: +46-8-7907164; Fax: +46-8-104879; E-mail: oed@theophys.kth.se.

0006-3495/00/07/426/08 $2.00

from the position of the carbon connecting the tails to the headgroup and the orientation by the average of vectors along the two tails. The lipids were randomly rotated, tilted up to 30 degrees, and given a 0.3-nm spread in the $z$-coordinate. The resulting structures were energy minimized with 500 steps of conjugate gradients. Finally, 23 simple point charge waters per lipid were added and the systems subjected to another 500 steps of energy minimization. To facilitate relaxation, the initial projected area/lipid was set to 0.65 $nm^2$, slightly higher than the experimental value (Nagle et al., 1996).

### Simulations

Each setup was first run for 50 ps with constant volume. Because the initial conformations had large fluctuations in lipid density, waters entering the hydrophobic core of 3.2-nm thickness during the first 25 ps were moved to the outside of the membrane. This run was followed by 50 ps of pressure coupling (Berendsen et al., 1984), scaling all directions separately to 1 atm with a time constant of 0.5 ps, corresponding to zero surface tension. In both simulations, the temperature of the system was scaled to 323 K with a time constant of 0.05 ps for water and lipids separately. A 1.0-nm cutoff was used for Lennard–Jones interactions and 1.8 nm for electrostatics. The long-range electrostatic contributions were updated every 10 steps. A timestep of 2 fs was used and all bond lengths were kept constant using the LINCS algorithm (Hess et al., 1997). The coupling time constants were subsequently doubled (still scaling temperature of lipids and water separately to 323 K and pressure separately in all directions to 1 atm), and the two larger systems run for 10 ns, the smallest one was extended to 60 ns. Scaling separately to atmospheric pressure in lateral and normal directions will produce an average zero surface tension. Because the coupling time constant is finite, there will still be small fluctuations in pressure and surface tension, but, when averaged over several nanoseconds, they are negligible. Because very slow relaxation and fluctuation modes were observed, the systems were allowed to equilibrate for 5 ns before data were collected for statistics. All simulations were performed with the molecular dynamics package GROMACS (Berendsen et al., 1995), using about 30,000 CPU hours for the largest system on an IBM SP2 parallel computer located at Center for Parallel Computers (PDC), Stockholm.

### Spatial spectral analysis

Spectral analysis was performed on coordinates with 2-ps spacing by fitting a grid to each monolayer, with the position of each lipid according to the definition above. Undulatory motions were defined by the average of the two grid layers and peristaltic (Israelachveli and Wennerström, 1992) by half the interlayer distance. The two-dimensional Fourier transform of this grid was computed to yield the $q$-space mode amplitudes, the square of which is the spectral intensity. The average intensity per mode was calculated by binning over wavenumbers. Due to the different mode densities in the systems, the result will be inversely proportional to the grid side squared. To compare the data in a single plot, the intensities of the two smaller system were scaled to correspond to the grid dimensions used for the largest system.

### Analysis in the temporal domain

Because of the slow dynamics in the systems, it is not possible to perform a full time-domain Fourier transform of the mode amplitude grid above. Even for the smallest system, the total simulation is only a few times the longest correlation times, and the mesoscopic region is only approached by the largest setup. Instead, we have studied the temporal dynamics by calculating the autocorrelations of mode amplitudes. For the undulatory modes, only data after 5 ns was used. The peristaltic modes are slightly slower, and the remaining 5–10-ns data do not entirely cover their period. To improve this thickness, data already from 2 ns were used, although it introduces a slight error resulting from the modes not being fully developed.

## THEORY OF MEMBRANE MOTION

### Undulatory motions

On the longest length scales, the bilayer can be modeled as a single surface, neglecting the membrane thickness. This applies to modes with wavelengths above a correlation length $\lambda_0 = 2\pi/q_0$, which is of the order of the membrane thickness. According to Safran (1994), the potential energy per unit projected area for such a mode is

$$E_{und}(x, y) = 0.5k_c|\nabla^2 u_{und}(x, y)|^2 + 0.5\gamma|\nabla u_{und}(x, y)|^2, \quad (1)$$

where the first term represents the cost of bending the membrane and the second one an external surface tension. In Fourier space, this simplifies to

$$E_{und}(q) = 0.5(k_c q^4 + \gamma q^2)u_{und}^2(q), \quad (2)$$

with $k_c$ the bending modulus and $\gamma$ the surface tension. Below the correlation length, the continuum picture is no longer valid; the monolayer motions will essentially be independent of each other, and the dominating processes single or collective temperature-excited motions of lipids (Lipowsky and Grotehans, 1993). The theoretical model for such protrusions predicts a restoring force similar to a microscopic surface tension, because the modes tend to increase true local surface area. It is important to note that this is only present on small length scales and does not interfere with the longer undulations. Otherwise, the term would have the properties of a macroscopic surface tension and dominate the dynamics as the wavelength increases. In practice, the transition from undulations to protrusions will be continuous, but we approximate it by separate equipartition in the two regions:

$$\langle u_{und}^2(q)\rangle = \frac{k_B T}{A} \times \begin{cases} (k_c q^4 + \gamma q^2)^{-1} & q < q_0 \\ (\gamma_p q^2)^{-1} & q > q_0, \end{cases} \quad (3)$$

where $A = L^2$ is the projected area of the system. Our simulations probe an ensemble with an average $\gamma \approx 0$, and the remaining fluctuations are negligible. Modes like these have been observed in simplified model systems of membranes (Goetz et al., 1999).

The total root mean square (RMS) amplitude of the undulatory modes in a system can be calculated as a function of the system size by summation over $q$. This is often replaced by an integral approximation, but, because the mode intensity increases fast for small $q$, this overestimates the result by more than 100% in the case of zero surface tension. We therefore use a numerical summation instead, giving

$$\langle u_{und}^2\rangle \approx \frac{k_B T A}{8.3\pi^3 k_c}, \quad (4)$$

where we have neglected the protrusions that will only contribute a constant factor in systems with a side larger

than the correlation length. The integral approximation yields a factor 4 instead of 8.3 in the denominator. The RMS amplitude is the square root of this expression.

From the potential energy in Eqs. 1 and 2, it is straightforward to construct a wave equation for a mode if we neglect the surrounding water. Unfortunately this turns out to be quite a poor approximation. A better model has to incorporate the finite viscosity and mass of the water damping the motions. Such an equation has been deduced in the limit of large wavelengths where the mass and thickness of the membrane are negligible (Kramer, 1971). The original model treats a membrane subject to surface tension, where the bending modulus contribution will be negligible, producing the dispersion relation,

$$2m\rho\omega^2 + (\gamma_0 - i\omega\gamma')q^3(q - m) = 0, \quad (5)$$

with $m = (q^2 - i\rho\omega/\eta)^{0.5}$, the complex eigenfrequency $\omega = \omega_0 - i\Gamma$, and $\rho$ and $\eta$ the density and viscosity of the damping water, respectively. The surface tension is designated $\gamma_0$ and surface viscosity $\gamma'$. It is easy to extend this to include the bending modulus, which will become important at low or zero surface tension. Looking at Eq. 3, we just replace $\gamma$ with $\gamma + k_c q^2$ in the dispersion relation. This has been found in excellent agreement with experiments (Hirn et al., 1999), but they have only been performed for wavelengths down to 1.8 $\mu$m, two orders of magnitude above our largest system.

For the $q$-values present in our systems, with negligible surface tension and surface viscosity, Eq. 5 simplifies to $\Gamma = k_c q^3/(4\eta)$, which represents strongly damped modes with a relaxation time $\tau = 2\pi/\Gamma$.

### Peristaltic motions

Thickness fluctuations can be treated analogous to the undulatory motions above, with the amplitude defined as half the deviation from the average membrane thickness, i.e., $u_{per} = (h - h_0)/2$. Also in this case, there will be an energy cost for bending the membrane sides, but the bending modulus $k_d$ need not be the same as above, depending on the details in the interactions between monolayers. There will also be a force restoring the thickness to its equilibrium value. To a first approximation, we assume it to be harmonic with constant $k_e$ and write the total energy per unit surface as:

$$E_{per}(x, y) = 0.5k_d|\nabla^2 u_{per}(x, y)|^2 + 0.5k_e u_{per}^2(x, y), \quad (6)$$

which in Fourier space becomes

$$E_{per}(q) = 0.5(k_d q^4 + k_e)u_{per}^2(q). \quad (7)$$

It is also possible to include a surface tension term, but, because it would be extremely small in our simulations due to the pressure scaling, we set $\gamma = 0$ to simplify the equations. Because the protrusions per definition is a process in the monolayers they should be of the same form irrespective of whether we are studying synchronous or asynchronous motions of the layers, and thus present also in peristaltic modes. Equipartitioning in the two regions, we get

$$\langle u_{per}^2(q)\rangle = \frac{k_B T}{A} \times \begin{cases} (k_d q^4 + k_e)^{-1} & q < q_0 \\ (\gamma_p q^2)^{-1} & q > q_0. \end{cases} \quad (8)$$

In principle, one could argue that the $k_e$ term should be present also at high $q$-values, but it would be small compared to the protrusions. Although the undulatory mode intensities increase for small $q$-values, the peristaltic ones thus tend asymptotically toward a constant value, determined by the force constant for keeping the monolayers at their equilibrium distance.

It is possible to calculate the total RMS amplitude for the peristaltic modes in Eq. 8 the same way as for undulatory modes. In this case, the integral approximation holds (at zero surface tension), producing,

$$\langle u_{per}^2\rangle = \frac{k_B T[\pi - 2\arctan(\sqrt{k_d/k_e}\,\pi^2/A)]}{8\pi\sqrt{k_d k_e}}. \quad (9)$$

The peristaltic spectral intensity holds for all modes with $q > 0$ in the system, where there is no net change in projected area of the system. In contrast to undulatory motions, however, we can also have a peristaltic mode with $q = 0$. Because the volume compressibility is at least an order of magnitude smaller than the area, this mode will be dominated by the cost of system area change. (The influence from $k_e$ is negligible in comparison.) Assuming zero volume compressibility, we have $\sigma_A h = \sigma_h A$. The projected area fluctuation can be deduced from ordinary ensemble theory (Allen and Tildesley, 1987), predicting

$$\sigma_A^2 = \frac{k_B T A}{K_A}, \quad (10)$$

where $K_A = A(\partial\gamma/\partial A)$ is the bilayer area compressibility modulus. We use this formula despite that the weak pressure coupling algorithm (Berendsen et al., 1984) does not produce a perfect NPT ensemble. For the practical purpose of evaluating a $K_A$, the limitations set by the length of equilibration and sampling are probably as or more severe than the inappropriateness of Eq. 10 in this situation.

## RESULTS

### Equilibrium properties

The development of projected area and volume per lipid during the whole 60-ns simulation of the smallest system is shown if Fig. 1 *A*, and the area of all three systems during the first 10 ns in Fig. 1 *B*. The average volume is 1.22 nm$^3$ in all cases, within a percent of the experimental value (Nagle and Wiener, 1988). This value is remarkably stable,

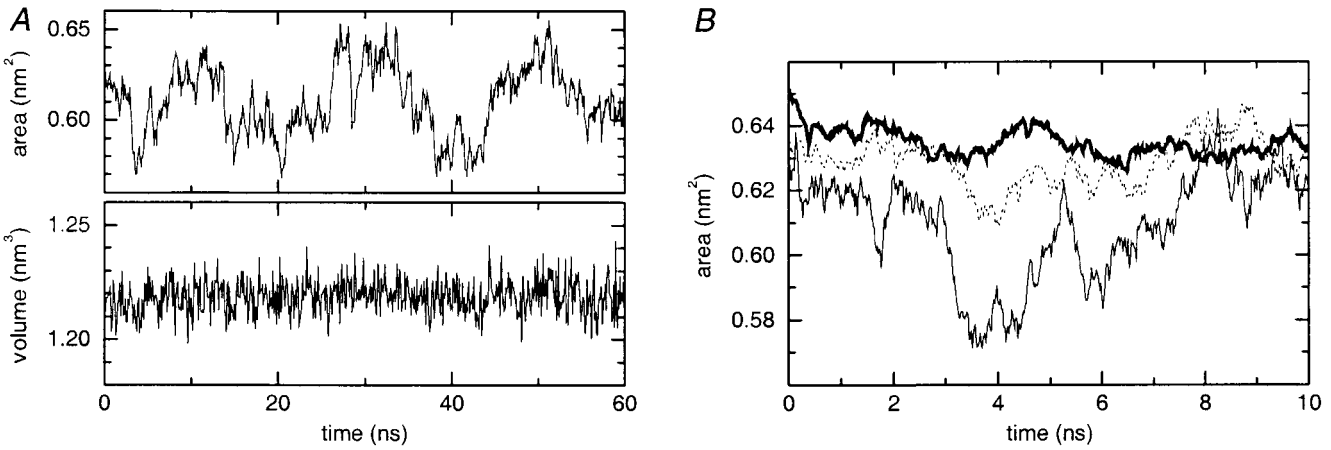


FIGURE 1 (*A*) Time development of projected area and volume per lipid for the smallest system during the 60-ns simulation. Although the volume is approximately constant, the area exhibits substantial fluctuations, with the longest period in the range of 20 ns; (*B*) Projected area/lipid for the small (*thin solid*), medium (*dotted*), and large system (*thick solid*) during the first 10 ns.

with a standard deviation of less than a percent and very short correlation times. The fluctuations in projected area/lipid are considerably larger, and the equilibrium value further exhibits a clear size dependence; 0.611, 0.630, and 0.633 $nm^2$, in order, smaller to larger system. This is displayed against inverse system size in Fig. 2 together with calculated standard errors. The data agree reasonably well with an inverse proportionality of the correction term, as anticipated from ensemble theory (see, e.g., Allen and Tildesley, 1987). Extrapolation gives $0.635 \pm 0.005$ $nm^2$ for an infinite system, which compares favorably with the experimental value $0.629 \pm 0.013$ $nm^2$ (Nagle et al., 1996). Using Eq. 10 for the observed fluctuations versus system size predicts $K_A = 300 \pm 50$ mN/m (dyn/cm) for the bilayer, in reasonable agreement with experiments on several similar types of lipids (Evans and Rawicz, 1990).

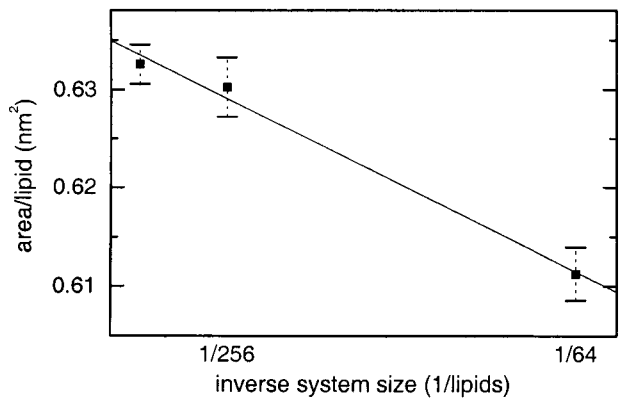


FIGURE 2 Average projected area per lipid versus system size. The error bars represent standard errors calculated from the area fluctuations and compensated for their time autocorrelation. The intercept of the solid line predicts the projected area for an infinite system to $0.635 \pm 0.005$ $nm^2$.

Values of $K_A$ in the same range have recently been calculated from smaller simulations (Feller and Pastor, 1999). With this value of $K_A$, the observed finite size effect on projected surface area for our smallest system could be corrected by applying a surface tension in the order of 10 mN/m (a factor of 3–4 smaller than the surface tensions used by Feller and Pastor (Feller et al., 1997; Feller and Pastor, 1999)), although this would change the dynamics of Eq. 5 to be dominated by external tension instead of bending modulus, increasing damping.

Figure 3 shows the time development of the largest system during the simulation with hydration waters removed for clarity. The development of mesoscopic dynamics is quite slow, partly because energy is introduced as short-scale fluctuations, which then must propagate to the longer modes through nonlinear effects. The motions are not fully developed until the last part of the simulation, but it is clear that there are dynamics on scales of several nanoseconds.

The resulting spectral distributions of mode intensities are presented in Fig. 4. Intensity is shown versus wavenumber for undulations in Fig. 4 *A* and peristaltic motions in Fig. 4 *B*. When scaled for the mode density, data from all three systems agree. The intensity of undulatory modes grows fast with wavelength (decreasing wavenumber $q$), as do the peristaltic modes for higher $q$-values. The latter modes initially show a decrease for small $q$-values, but this is due to their slower initial growth. For the three smallest $q$-values in the largest system, we have therefore separately plotted the data from 5–7.5 ns (*crosses*) and 7.5–10 ns (*filled squares*). This behavior comes from the energy being introduced through the shorter modes, and the system has thus not yet reached equilibrium. It is still possible to estimate the equilibrium value, though, and the transition region.

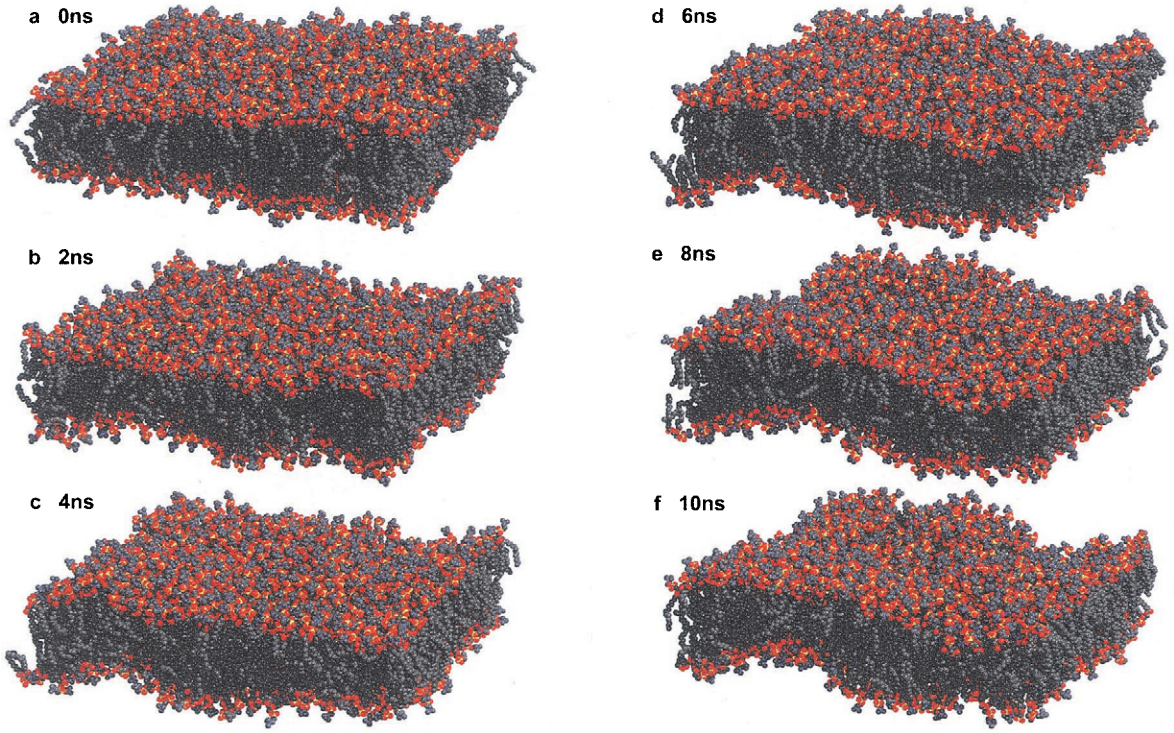


FIGURE 3 Development of undulatory and peristaltic modes for the largest system. Initially, there is a considerable roughening of the surfaces with vertical displacement of lipids. From 4 ns, we also see substantial long-range undulatory and peristaltic modes, but they are not fully developed until the last part of the trajectory. (Pictures produced with Raster3D (Marritt and Bacon, 1997))

## Undulatory motions

For the undulatory bending modes, we observe two distinct kinds of dynamics on different scales. At $q$-values smaller than 1.5 $nm^{-1}$, corresponding to wavelengths larger than the membrane thickness, mesoscopic undulations dominate. These have a spectral distribution proportional to $q^{-4}$ and involve more than 50 lipids in the membrane. On intermediate scales (1.5–4 $nm^{-1}$), the spectral distribution behaves as $q^{-2}$. These modes might be the collective lipid protrusions suggested from theory (Lipowsky and Grotehans, 1993), in which case they should occur independently in the

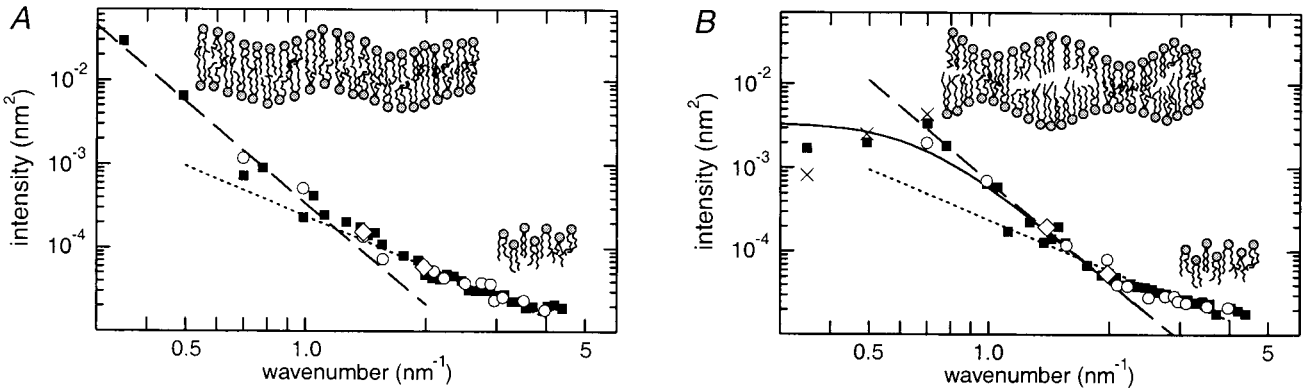


FIGURE 4 Spectral intensity per mode versus wave vector for small (*diamond*), medium (*circle*), and large system (*square*). (*A*) Undulatory relaxations. The dashed line is the undulatory $q^{-4}$ modes determined by bending modulus, whereas the dotted line describes protrusion modes from the roughening of the molecular surface at higher wave vector, showing a $q^{-2}$ behavior; (*B*) Peristaltic oscillations. The three lowest modes are still increasing after 5 ns, so these have been divided into 5–7.5-ns data (*cross*) and 7.5–10-ns data (*square*). The solid line is obtained from Eq. 8 with $K_A$ and $k_d$ fitted. The dashed curve represents the high-$q$ modes determined by bending energy, proportional to $q^{-4}$ and the dotted protrusion modes.

two monolayers involving less than 25 lipids. Finally, for $q$-values above 4 $nm^{-1}$ (about two interlipid distances), the spectrum disappears into noise, due to the definition of lipid position from a single atom.

Fitting for low values of $q$ in Fig. 4 *A* shows good conformance to $q^{-4}$ for $q < 1$ nm (*dashed line*), and we estimate the bending modulus to $4 \times 10^{-20}$ J, in good agreement with experiments (Evans and Rawicz, 1990) on similar membranes reporting $k_c \approx 5 \times 10^{-20}$ J. Other sources (Duwe and Sackmann, 1990) indicate values 2–3 times larger for cellular membranes. The protrusion modes fit the intermediate-$q$ data with $\gamma_p \approx 50$ mN/m (*dotted line*).

The dotted and dashed curves in Fig. 5 *A* show the time autocorrelation of the two longest undulatory modes in the largest system. The damping behavior predicted by the dispersion relation in Eq. 5 with the $k_c$ above and $\eta = 1$ mPas for water is drawn solid. At short times, the decay is slightly faster than predicted, but, considering that the equation is deduced for much larger wavelengths in the limit of negligible thickness, the simulation results are in very good agreement with the mesoscopic model. The relaxation time $\tau$ of the longest mode is approximately 2 ns and of the next longest mode 0.7 ns. From this, we have a uniform description of membrane dynamics over 5 orders of spatial magnitude, from 0.25 mm macroscopic wavelengths down to the membrane thickness, or even the interlipid distance if we include the protrusions regime. The corresponding periods or relaxation times cover $10^{-4}$–$10^{-10}$ s.

## Peristaltic motions

The intensity of the thickness oscillations shown in Fig. 4 *B* can also be characterized by different regions. For small $q$, it cannot increase indefinitely, but is limited by the equilibrium membrane thickness. It tends asymptotically toward a constant value for small $q$ and does not change much below $q \approx 0.5$ $nm^{-1}$ (modes involving more than 400 lipids). There are $q^{-4}$ bending modes involving 50–400 lipids in the region $q = 0.5$–$1.5$ $nm^{-1}$, and protrusion modes for $q = 1.5$–$4$ $nm^{-1}$. Finally, for $q > 4$ $nm^{-1}$ (below two interlipid distances), the spectrum is dominated by noise.

Fitting to the intermediate $q$-values of Fig. 4 *B* gives $k_d = 2 \times 10^{-20}$ J. The factor 2 difference between $k_d$ and $k_c$ indicates that it is slightly easier to bend monolayers anticorrelated, changing thickness than to bend them correlated producing undulations. From the low-$q$ region, we estimate the value of $k_e$ to $4 \times 10^{-21}$ J/$nm^4$. The peristaltic bending modes extend to wavenumbers about twice as large as for the undulatory ones. The protrusions modes are identical to those in the bilayer, supporting the view that they occur independently in the two monolayers.

The $q = 0$ peristaltic mode has an intensity of $1.2 \times 10^{-4}$ $nm^2$ for all three systems when scaled to the mode density of the largest. This gives $K_A \approx 250 \pm 50$ mN/m, which is compatible with the value obtained directly from area fluctuations and confirms the negligible volume compressibility.

## Area dependence in simulations

A statistically better way of determining bending modulus is to use the system size dependence of total surface RMS fluctuations. This also provides a direct picture of size effects. Displacements can be calculated directly from simulations and compared with the sum over modes from Eqs. 3 and 8; the results are presented in Fig. 6. The undulatory RMS amplitude increases linearly with size, whereas the peristaltic reaches a constant value. Fitting to the sum in Eq. 4 confirms the bending modulus to $k_c = 4.0 \times 10^{-20}$ J. The predicted sum over peristaltic modes in Eq. 9 also agrees well with the corresponding observed displacement, using $k_e = 4 \times 10^{-21}$ J/$nm^4$ and $k_d = 2 \times 10^{-20}$ J.

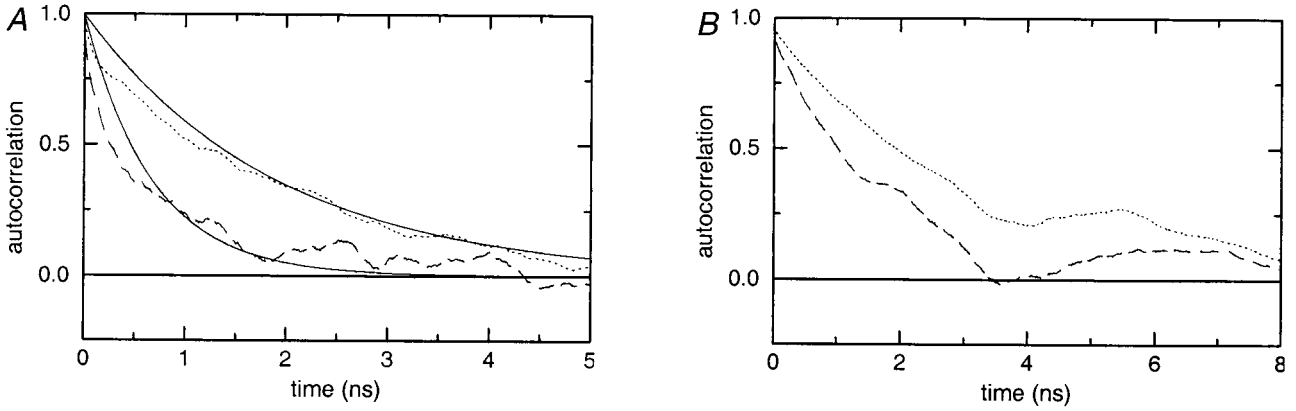


FIGURE 5 Time autocorrelation functions of single modes. (*A*) The two lowest undulatory modes, with $q = 0.35$ $nm^{-1}$ (*dotted*) and $q = 0.5$ $nm^{-1}$ (*dashed*). The solid lines are the relaxations predicted from Eq. 5; (*B*) Peristaltic motions for the same wavenumbers, note the different scale. The process is a combination of relaxation and oscillation with a period in the range of 6 ns.

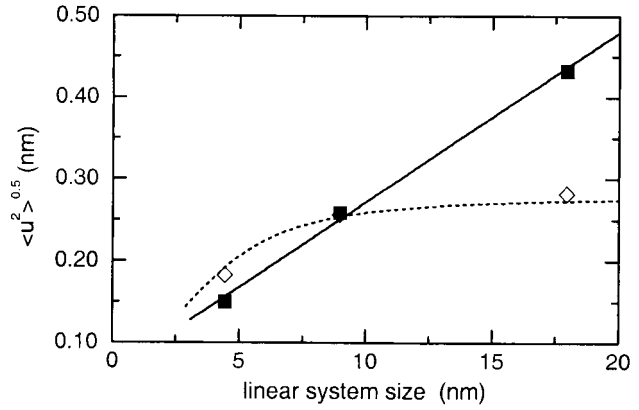


FIGURE 6 Total RMS amplitude of undulatory (*square*) and peristaltic (*diamond*) modes versus system size. The solid line is a linear fit to the sum of modes in Eq. 4, whereas the dotted line corresponds to the sum in Eq. 9.

We further see that, for systems smaller than ~10 nm, the thickness fluctuations, and thereby also the coupled fluctuations in projected area, have not reached their mesoscopic value. Of course there is also a size dependence in the undulatory modes, but these are not strongly coupled to the area. This is easily checked by comparing correlations between the entities. In Fig. 7 we have plotted normalized 1-ns running averages of the projected area fluctuations versus intensities of peristaltic and undulatory modes. There is a clear correlation between large areas and high peristaltic intensity. This is actually quite reasonable, because the peristaltic modes incur relative motions of the tails in the two monolayers. Any such motions will increase the disorder in the hydrophobic region, and high order is tightly coupled to low projected area/lipid (Nagle, 1993; Berger et al., 1997). This would explain the too low projected area in the smallest system by the decreasing RMS peristaltic amplitude at short lengthscales. The corresponding modes are present in all systems, but their relative weight increases with decreasing system size.

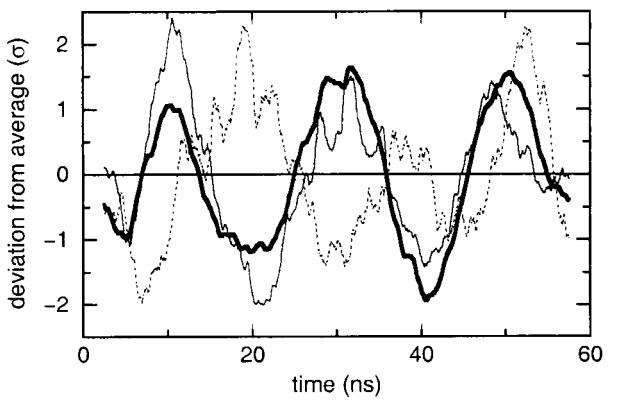


FIGURE 7 Correlation of projected area fluctuations (*thick solid*) with peristaltic (*thin solid*) and undulatory (*dotted*) modes for the small system. One-nanosecond running averages of the deviations from the time average value in units of standard deviations are shown versus time during the simulation. The average correlation coefficient of projected area with peristaltic modes is 0.83 and with undulatory modes −0.39.

The correlation with undulatory modes is considerably lower, and negative. If these modes were the cause of the area discrepancy, we would thus have observed a lower projected area when the undulatory intensity increases with increasing system size, in contrast to the observations.

## Area compressibility

The value 250–300 mN/m obtained for the area compressibility of the bilayer is actually a combination of several phenomena. First, we have an intrinsic compressibility $K_A^{int}$ from changing the true local area of a resting bilayer, but there is also a second contribution $K_A^{und}$ from the ability of the system to change its projected area by altering the intensity of undulations at constant true local area. Because the processes occur in parallel, essentially independent of each other, they should combine as

$$\frac{1}{K_A} = \frac{1}{K_A^{int}} + \frac{1}{K_A^{und}}. \tag{11}$$

The volume compressibility will also contribute a small area compressibility, $K_A^{vol}$. The volume compressibility has been calculated to $4.5 \times 10^{-5}$ atm$^{-1}$ from simulations (Berger et al., 1997) and $4–5 \times 10^{-5}$ atm$^{-1}$ from experiments (Braganza and Worcester, 1986). These values correspond to an area compressibility $K_A^{vol}$ that is in the order $10^4$ mN/m and thus negligible. It is of some interest to relate the second, undulatory, contribution to solid mechanics models for thin films (Goetz et al., 1999). In these, the bending modulus relates to area compressibility and membrane thickness $h$ through the relation

$$K_A^{und} = \frac{48k_c}{h^2}, \tag{12}$$

where $h$ is the effective thickness of the membrane. With the $k_c = 4 \times 10^{-20}$ J observed in the simulations and $h = 3.5$ nm, this gives a $K_A^{und} = 160$ mN/m, which is the right order of magnitude but at least a factor 2 too small to account for the $K_A$ observed in the simulations. This indicates that the model in Eq. 12 is qualitatively but not quantitatively correct.

This combination of processes means that the actual value of $K_A$ observed in an experiment or simulation will depend on the conditions at which this is performed. E.g., applying a surface tension to the system will reduce undulations and thereby the undulatory contribution to $K_A$.

## SUMMARY

We have found the collective dynamics in lipid bilayers to be a combination of several processes on different scales.

From interlipid distances up to a handful of molecules, the predominant motions are single or collective protrusions of lipids in each monolayer, described by an effective microscopic surface tension $\gamma_p = 50$ mN/m.

At larger lengthscales, collective undulations and peristaltic motions dominate the dynamics, and it is possible to model the layers as continuous surfaces. The peristaltic modes are anticorrelated motions of the two monolayers and described by a bending modulus $k_d = 2 \times 10^{-20}$ J. On scales larger than the membrane thickness, there are undulatory correlated motions of the monolayers, described by a bending modulus $k_c = 4 \times 10^{-20}$ J.

When wavelengths 3–4 times the membrane thickness are reached, the peristaltic modes have attained their mesoscopic value, determined by the force constant keeping the monolayers at their equilibrium distance, $k_e = 4 \times 10^{-21}$ J/nm$^4$. At even larger scales, the relative importance of the peristaltic dynamics will diminish, and the bilayer behave more like a single surface.

The longer undulatory mode dynamics is in very good agreement with a mesoscopic dispersion relation (Kramer, 1971). For the wavenumbers accessible to simulations, it simplifies to $\Gamma = k_c q^3/(4\eta)$, predicting strongly damped modes with a 2-ns relaxation time at $\lambda = 20$ nm. Together with experimental results (Hirn et al., 1999), this gives a uniform description of membrane dynamics covering 5–6 orders of magnitude in both space and time.

This work was supported with computing resources by the Swedish Council for Planning and Coordination of Research (FRN) and Parallelldatorcentrum (PDC), Royal Institute of Technology.

## REFERENCES


Allen, M. P., and D. J. Tildesley. 1987. Computer Simulation of Liquids. Clarendon Press, Oxford. 43–54.

Berendsen, H. J. C., J. P. M. Postma, A. DiNola, and J. R. Haak. 1984. Molecular dynamics with coupling to an external bath. *J. Comp. Phys.* 81:3684–3690.

Berendsen, H. J. C., D. van der Spoel, and R. van Drunen. 1995. GROMACS: a message-passing parallel molecular dynamics implementation. *Comp. Phys. Comm.* 91:43–56.

Berger, O., O. Edholm, and F. Jähnig. 1997. Molecular dynamics simulation of a fluid bilayer of dipalmitoylphosphatidylcholine at dull hydration, constant pressure and constant temperature. *Biophys. J.* 72: 2002–2013.

Bloom, M., E. Evans, and O. G. Mouritsen. 1991. Physical properties of the fluid lipid-bilayer component of cell membranes: a perspective. *Quart. Rev. Biophys.* 24:293–397.

Braganza, L. F., and D. L. Worcester. 1986. Structural changes in lipid bilayers and biological membranes caused by hydrostatic pressure. *Biochemistry.* 25:7484–7488.

Chiu, S., M. Clark, V. Balaji, S. Subramaniam, H. Scott, and E. Jakobsson. 1995. Incorporation of surface tension into molecular dynamics simulation of an interface: a fluid phase lipid bilayer membrane. *Biophys. J.* 69:1230–1245.

Duwe, H. P., and E. Sackmann. 1990. Bending elasticity and thermal excitations of lipid bilayer vesicles: modulation by solutes. *Physica A.* 163:410–428.

Egberts, E., and H. J. C. Berendsen. 1988. Molecular dynamics simulation of a smectic liquid crystal with atomic detail. *J. Chem. Phys.* 98: 1712–1720.

Evans, E. 1991. Entropy-driven tension in vesicle membranes and unbinding of adherent vesicles. *Langmuir.* 7:1900–1908.

Evans, E., and W. Rawicz. 1990. Entropy driven tension and bending elasticity in condensed-fluid membranes. *Phys. Rev. Lett.* 64: 2094–2097.

Feller, S. E., and R. W. Pastor. 1996. On simulating lipid bilayers with and applied surface tension: periodic boundary conditions and undulations. *Biophys. J.* 71:1350–1355.

Feller, S. E., and R. W. Pastor. 1999. Constant surface tension simulations of lipid bilayers: the sensitivity of surface areas and compressibilities. *J. Chem. Phys.* 111:1281–1287.

Feller, S. E., R. M. Venable, and R. W. Pastor. 1997. Computer simulation of a DPPC phospholipid bilayer: structural changes as a function of molecular surface area. *Langmuir.* 13:6555–6561.

Gennis, R. B. 1989. Biomembranes: Molecular Structure and Function. Springer, New York.

Goetz, R., G. Gompper, and R. Lipowsky. 1999. Mobility and elasticity of self-assembled membranes. *Phys. Rev. Lett.* 82:221–224.

Hess, B., H. Bekker, H. J. C. Berendsen, and J. G. E. M. Fraaije. 1997. LINCS: a linear constraint solver for molecular simulations. *J. Comp. Chem.* 18:1463–1472.

Hirn, R., R. Benz, and T. M. Bayerl. 1999. Collective membrane motions in the mesoscopic range and their modulation by the binding of a monomolecular protein layer of streptavidin studied by dynamic light scattering. *Phys. Rev. E.* 59:5987–5994.

Israelachveli, J. N., and H. Wennerström. 1990. Hydration or steric forces between amphiphilic surfaces? *Langmuir.* 6:873–876.

Israelachveli, J. N., and H. Wennerström. 1992. Entropic forces between amphiphilic surfaces in liquids. *J. Phys. Chem.* 96:520–531.

Jorgensen, W., and J. Tirado-Rives. 1988. The OPLS potential functions for proteins. Energy minimizations for crystals of cyclic peptides and crambin. *J. Am. Chem. Soc.* 110:1657–1666.

König, S., and E. Sackmann. 1996. Molecular and collective dynamics of lipid bilayers. *Cur. Opin. Colloid Interface Sci.* 1:78–82.

Kramer, L. 1971. Theory of light scattering from fluctuations of membranes and monolayers. *J. Chem. Phys.* 55:2097–2105.

Lipowsky, R., and S. Grotehans. 1993. Hydration vs. protrusion forces between lipid bilayers. *Europhys. Lett.* 23:599–604.

Marritt, E. A., and D. J. Bacon. 1997. Raster3D photorealistic molecular graphics. *Meth. Enzymol.* 277:505–524.

Nagle, J. F. 1993. Area/lipid of bilayers from NMR. *Biophys. J.* 64: 1476–1481.

Nagle, J. F., and M. C. Wiener. 1988. Structure of fully hydrated bilayer dispersions. *Biochem. Biophys. Acta.* 942:1–10.

Nagle, J. F., R. Zhang, S. Tristram-Nagle, W. Sun, H. Petrache, and R. M. Suter. 1996. X-ray structure determination of fully hydrated $L_\alpha$ phase dipalmitoylphosphatidylcholine bilayers. *Biophys. J.* 70:1419–1431.

Pastor, R. W. 1994. Computer simulations of lipid bilayers. *Curr. Opin. Struct. Biol.* 4:486–492.

Ryckaert, J. P., G. Ciccotti, and H. J. C. Berendsen. 1977. Numerical integration of the Cartesian equations of motion of a system with constraints; molecular dynamics of *n*-alkanes. *J. Comput. Phys.* 23: 327–341.

Safran, S. A. 1994. Statistical Thermodynamics of Surfaces, Interfaces, and Membranes. Addison-Wesley, Reading, MA.

Seelig, J., and A. Seelig. 1974. Dynamic structure of fatty acyl chains in a phospholipid bilayer measured by DMR. *Biochemistry.* 13:4839–4845.

Tieleman, D. P., S.-J. Marrink, and H. J. C. Berendsen. 1997. A computer perspective of membranes: molecular dynamics studies of lipid bilayer systems. *Biochim. Biophys. Acta.* 1331:235–270.

Tu, K., D. J. Tobias, J. K. Blasie, and M. L. Klein. 1996. Molecular dynamics investigation of the structure of a fully hydrated gel-phase dipalmitoylphosphatidylcholine bilayer. *Biophys. J.* 70:595–608.